

Optimal design of catalytic converters for minimizing cold-start emissions

Karthik Ramanathan^a, David H. West^b, Vemuri Balakotaiah^{a,*}

^aDepartment of Chemical Engineering, University of Houston, Houston, TX 77204-4004, USA

^bThe Dow Chemical Company, Freeport, TX 77541, USA

Available online 28 September 2004

Abstract

A transient one-dimensional two-phase model is used to obtain an explicit light-off criterion and to estimate the transient time and cumulative cold-start emissions from a catalytic monolith for the case of nonuniform catalyst loading. The light-off criterion can predict the nature of ignition (front-end, middle or back-end). For a fixed amount of metal loading, redistribution of the catalyst appropriately (with more catalyst near the inlet) favors front-end ignition in the monolith and reduces the cumulative cold-start emissions substantially. It is also found that there exists an optimal washcoat thickness and/or metal loading, above which the performance of the converter does not improve significantly while below this optimum, the transient time and cumulative emissions can be reduced by increasing the washcoat thickness or metal loading. For the case of front-end ignition, it is also found that the total transient time is the sum of ignition and the front-propagation times. We present analytical expressions for both these times and show how they may be used to estimate cumulative cold-start emissions. Numerical simulations validate the analytical design criteria presented. Finally, some strategies for minimizing cumulative cold-start emissions are discussed.

© 2004 Elsevier B.V. All rights reserved.

Keywords: Catalytic converter; Monolith reactor; Nonuniform catalyst loading; Cold-start emissions; Cumulative emissions

1. Introduction

The monolithic reactor is the most common and widely used catalytic reactor today, with an estimated 600 million units in use in automobiles alone. It also finds applications in the oxidation of VOCs, catalytic partial oxidation of hydrocarbons and removal of NO_x from power plant and furnace exhaust gases. The monolith reactor is a large number of small, long channels of diameter 0.5–2 mm and length 5–20 cm in parallel through which the reacting fluid flows. The catalyst (containing the precious metals such as Pt, Pd and/or Rh) is deposited on the walls of the monolith channels as a porous washcoat. Due to the small channel dimensions, the flow is laminar in most cases with Reynolds numbers in the range 100–1000. The reactants (CO, HC and/or NO) enter the monolith channel and react at the catalyst sites within the porous washcoat. Catalytic converters used in automobiles require designs that lead to

very low cold-start emissions. When the converter is cold, the entering reactants leave the reactor unreacted and the exit concentration is very high during this period. At steady-state, when the converter is ignited and hot, the exit concentration reduces. To minimize the cold-start emissions, we need to minimize the transient time as well as increase the steady state conversion. The complex coupling between the various physical and chemical processes involved in catalytic converters and the large number of design and operating parameters makes it difficult to simulate the behavior in the multidimensional parameter space without sufficient theoretical analysis and guidance. The focus of this work is to present such analysis and to obtain design criteria that may be used to minimize cumulative cold-start emissions.

2. Literature review

There is extensive literature during the last three decades describing both the experimental and modeling aspects of

* Corresponding author. Tel.: +1 713 743 4318; fax: +1 713 743 4323.
E-mail address: bala@uh.edu (V. Balakotaiah).

Nomenclature

$a_c(x)$	catalyst distribution function along the channel length
A_r	frequency/pre-exponential factor
C	concentration (mol/m ³)
$C_{m,in}$	inlet fluid concentration
D_e	effective diffusivity of reactant in the washcoat
D_m	diffusion coefficient in the fluid phase
E	activation energy
E_{cum}	cumulative emissions (mol)
$h(x)$	position-dependent heat transfer coefficient
$k_c(x)$	position-dependent mass transfer coefficient
k_f	fluid thermal conductivity
k_v	first-order rate constant per unit washcoat volume
k_w	solid thermal conductivity
L	length of the monolith channel
M_w	molecular weight
N	number of channels in the monolith
N_R	number of reactions
$Nu(z)$	Nusselt number
Pe_h	heat Peclet number
R_g	universal gas constant
R_Ω	one-fourth the channel hydraulic diameter
$Sh(z)$	Sherwood number
t	time
T	fluid temperature
$T_{f,in}$	inlet fluid temperature
\bar{u}	average fluid velocity in the channel
W	mass flow rate
x	coordinate along the length of the channel
y	transverse coordinate

Greek letters

α_1	numerical constant to determine exit conversion
δ_c	effective thickness of the washcoat
δ_s	half thickness of the support
δ_w	effective wall thickness
η	effectiveness factor
φ	washcoat Thiele modulus

Subscripts and superscripts

f	fluid phase and/or cup-mixing
m	cup-mixing
s	solid phase

monolith reactors. Articles by Hegedus [1], Heck et al. [2], Young and Finlayson [3] and Boersma et al. [4] are amongst the first that describe both the experimental and modeling work on catalytic monoliths. Review articles by Cybulski and Moulijn [5], Groppi et al. [6] and books by Becker and Pereira [7], Hayes and Kolaczowski [8] summarize the recent progress. Groppi et al. [9] and Tronconi and Forzatti

[10] had done a comparison of the lumped and distributed models used for modeling catalytic monoliths.

The transient behavior of catalytic monoliths was also studied widely in the literature. Oh and Cavendish [11] presented transient calculations on catalytic monoliths using a one-dimensional two-phase model. Please et al. [12] and Kirchner and Eigenberger [13], studied the light-off and dynamic behavior of catalytic converters, respectively. Leighton and Chang [14], Keith et al. [15] analyzed the propagation of the ignition front using a two-phase model with constant transfer coefficients with very low or zero solid conduction. Kirchner and Eigenberger [16] suggested using an electrically preheated catalyst to improve the cold-start performances. The models considered by these authors assume that the washcoat diffusion is negligible but it was found that the washcoat diffusion does have a profound influence on the light-off behavior [17].

Some studies also focused on the influence of nonuniform catalyst loading on the performance of catalytic monoliths. Oh and Cavendish [11] studied the effect of linearly increasing and decreasing activity profiles. Psyllos and Philippopoulos [18] observed that a parabolic activity distribution (decreasing from entrance to exit) reduces the warm-up time. Cominos and Gavrilidis [19] found that an exponentially decreasing activity profile favors light-off near the inlet and also helps in alleviating the temperature gradients. Ramanathan et al. [20] also analyzed the steady-state behavior of catalytic monoliths with nonuniform catalyst distribution.

Most of these earlier studies were confined to specific cases and/or uniform catalyst distribution and a systematic analysis of the transient behavior was lacking. Tronci et al. [21] found that a monotonically decreasing or a two-zone catalyst distribution with more catalyst near the inlet leads to the minimal cold-start emissions. This work concentrated on obtaining the optimal activity profile for a specific set of parameters and considered the case of no washcoat diffusion. Ramanathan et al. [22] presented a detailed analysis of the effect of various design and operating variables on the cumulative emissions and also suggested ways to obtain optimal designs. A systematic study of the transient behavior of catalytic monoliths analyzing the different processes involved (kinetically controlled, ignition, front propagation, mass transfer controlled regime) is currently lacking. Such a study helps in obtaining optimal design of catalytic monoliths to reduce the cold-start emissions.

3. Mathematical model

Depending on the level of detail included, the mathematical models for catalytic monoliths may be classified into four groups. The first class of models is the pseudohomogeneous type where the temperature and concentration

difference between the fluid and the solid is assumed to be negligible and a single equation (one for each species and an energy balance) for both the phases is written. This type of model cannot predict the different regimes (kinetically controlled and mass transfer controlled) that usually exist in these catalytic reactors. Also, these models do not capture many of the observed qualitative features of the catalytic monolith reactor. The next level model is the two-phase model, which is the most widely used model for these reactors. Here, a separate equation is written for both the solid and the fluid phases and these are obtained by averaging the full convection–diffusion–reaction equations in the transverse direction. These models, which have been tested extensively in the past thirty years, capture all the qualitative features of the reactor and the quantitative predictions are also quite accurate. These can also predict the different regimes (kinetically controlled and mass transfer controlled) and the ignition behavior accurately. The two-phase model, also helps in obtaining analytical results which sometimes are of great practical importance. The third level of models extend the two-phase model by replacing the overall kinetics by the detailed chemistry of the reactions at the catalytic sites (micro-kinetics). Just like the two-phase model, these capture the qualitative and quantitative features of the monolith reactor quite accurately. The computational time for these models is much higher compared to the two-phase model with overall kinetics because of the inclusion of the detailed chemistry coupled with the fluid flow equations. The fourth level of model is the complete convection–diffusion–reaction equation with detailed chemistry. While these can capture the quantitative and qualitative features accurately, these are not practical to use (especially when the objective is to explore the parameter space and evaluate various designs) because of the computational time involved in solving a large number of partial differential equations.

In this work, we use the two-phase model with overall kinetics and assume a single reaction. The model is the same as that developed by Ramanathan et al. [17] and is given by

$$\bar{u} \frac{\partial C_m}{\partial x} = -\frac{k_c(x)}{R_\Omega} (C_m - C_s) \quad (1)$$

$$\bar{u} \rho_f c_{pf} \frac{\partial T_f}{\partial x} = -\frac{h(x)}{R_\Omega} (T_f - T_s) \quad (2)$$

$$k_c(x) (C_m - C_s) = a_c(x) R_v(C_s, T_s) \delta_c \eta \quad (3)$$

$$\delta_w \rho_w c_{pw} \frac{\partial T_s}{\partial t} = \delta_w k_w \frac{\partial^2 T_s}{\partial x^2} + (-\Delta H_R) a_c(x) R_v(C_s, T_s) \delta_c \eta - h(x) (T_s - T_f) \quad (4)$$

$$D_e \frac{\partial^2 C}{\partial y^2} = a_c(x) R_v(C, T_s), \quad 0 < y < \delta_c \quad (5)$$

$$C = C_s \quad \text{at } y = 0, \quad \frac{\partial C}{\partial y} = 0 \quad \text{at } y = \delta_c \quad (6)$$

$$\eta \delta_c a_c(x) R_v(C_s, T_s) = -D_e \left. \frac{\partial C}{\partial y} \right|_{y=0} \quad (7)$$

$$C_m = C_{m,in}(t), \quad T_f = T_{f,in}(t) \quad \text{at } x = 0 \quad (8)$$

$$\frac{\partial T_s}{\partial x} = 0 \quad \text{at } x = 0, L \quad (9)$$

$$T_s(x, t = 0) = T_{s0}(x) \quad (10)$$

The fluid and solid phase species and energy balances are given by Eqs. (1)–(4). Eqs. (5) and (6) describe the reactant concentration profile in the washcoat while Eq. (7) gives the washcoat effectiveness factor (η). Eqs. (8)–(10) define the boundary and initial conditions. Here, x and t represent the axial coordinate along the channel and time, respectively. T_f and C_m represent the cup-mixing temperature and concentration in the fluid phase while T_s and C_s denote the solid phase temperature and the reactant concentration at the fluid–solid interface. $a_c(x)$ is the normalized activity (catalyst distribution) profile along the channel ($(1/L) \int_0^L a_c(x) dx = 1$) and $R_v(C, T)$ is the intrinsic reaction rate per unit volume of washcoat [$R_v(C, T) = R_s(C, T) S_v$, where $R_s(C, T)$ is the rate based on unit internal surface area and S_v is the internal surface area per unit washcoat volume.] R_Ω is the effective transverse (diffusion or conduction) length scale ($R_\Omega = A_\Omega / P_\Omega$; A_Ω = channel cross-sectional area open to flow, P_Ω = channel perimeter open to flow. $R_\Omega = d_h/4$, d_h = channel hydraulic diameter), δ_c is the effective washcoat thickness (defined as the volume of the washcoat over the fluid–washcoat interfacial area) and δ_w is the effective wall thickness (defined as the sum $\delta_s + \delta_c$, where δ_s is the half-thickness of the solid wall without washcoat). In Eqs. (5)–(7), y is the local distance (from fluid–washcoat interface) coordinate in the washcoat and η is the internal effectiveness factor in the washcoat.

The coefficients of the accumulation and conduction terms in the solid-phase energy balance could be written more explicitly as

$$\delta_w \rho_w c_{pw} = [\delta_c \rho_c c_{pc} + \delta_s \rho_s c_{ps}] \quad (11)$$

$$\delta_w k_w = [\delta_c k_c + \delta_s k_s], \quad (12)$$

where the subscript s (c) refers to the support (catalyst or washcoat). D_e and D_m are the effective diffusivities of the reactant in the washcoat and fluid phase, respectively. The other symbols have their usual meaning and are explained in the notation section.

The following expressions describe the local heat and mass transfer coefficients in the monolith channel when the

flow is laminar and fully developed at the entrance:

$$Sh_{\Omega}(x) = \frac{k_c(x)R_{\Omega}}{D_m} = \begin{cases} 0.82 \left(\frac{R_{\Omega}^2 \bar{u}}{x D_m} \right)^{1/3} & 0 < x < \frac{R_{\Omega}^2 \bar{u}}{D_m} \left(\frac{3.28}{Sh_{H_1, \infty}} \right)^3 \\ \frac{Sh_{H_1, \infty}}{4} & x \geq \frac{R_{\Omega}^2 \bar{u}}{D_m} \left(\frac{3.28}{Sh_{H_1, \infty}} \right)^3 \end{cases} \quad (13a)$$

$$Nu_{\Omega}(x) = \frac{h(x)R_{\Omega}}{k_f} = \begin{cases} 0.82 \left(\frac{R_{\Omega}^2 \bar{u} \rho_f c_{pf}}{x k_f} \right)^{1/3} & 0 < x < \frac{R_{\Omega}^2 \bar{u} \rho_f c_{pf}}{k_f} \left(\frac{3.28}{Nu_{H_1, \infty}} \right)^3 \\ \frac{Nu_{H_1, \infty}}{4} & x \geq \frac{R_{\Omega}^2 \bar{u} \rho_f c_{pf}}{k_f} \left(\frac{3.28}{Nu_{H_1, \infty}} \right)^3 \end{cases} \quad (13b)$$

A detailed theoretical basis for the above correlations is presented elsewhere [23,24]. The above model is valid for any arbitrary channel shape and washcoat profile, provided $\delta_c \ll R_{\Omega}$. (In practice, this condition is satisfied since δ_c is around 10–50 μm while R_{Ω} is around 200–300 μm). Table 1 gives the asymptotic constants for some common channel shapes. The second column of the table defines the effective diffusion length, R_{Ω} for the channel. The third column gives the asymptotic Nusselt/Sherwood number for a wall catalyzed reaction for the case of slow reaction (Nu_{H_2}/Sh_{H_2}). The fourth column gives the Nusselt/Sherwood number for the case of slow reaction but with uniform concentration/temperature along the perimeter (Nu_{H_1}/Sh_{H_1}). The fifth column of the table gives the asymptotic Sherwood (Nusselt) number for the case of fast reaction (or constant temperature/concentration boundary condition). The sixth column gives the friction factor while the last column gives the Fourier weight for predicting the conversion in the mass transfer controlled regime. Some numerical values listed in this table are taken from Shah and London [25] while others are computed using the procedure outlined by Balakotaiah and West [24]. The asymptotic Sherwood/Nusselt numbers and friction factors given in Table 1 are for channels with very thin washcoat. When the addition of washcoat changes the geometrical shape (and the flow area) of the channel, these constants have to be modified accordingly.

In this work, we shall use first-order kinetics ($R_v(C, T) = k_v(T)C = A_r \exp(-E/R_g T)C$, A_r is the frequency/pre-exponential factor having units of inverse time) and assume that the reaction is exothermic. This case allows us to obtain some general results (valid for monotone kinetics) and

qualitative trends that describe the transient performance of the monolith. [The generalization of the results to nonlinear kinetics and multiple reactions is discussed in the last section.] For the case of first-order reaction, Eqs. (5)–(7) can be solved analytically and the effectiveness factor η is given by

$$\eta = \frac{\tanh(\delta_c \sqrt{k_v(T_s) a_c(x)/D_e})}{(\delta_c \sqrt{k_v(T_s) a_c(x)/D_e})} \quad (14)$$

The solid phase concentration can be eliminated using Eq. (3) and is related to the fluid phase concentration by

$$C_s = \frac{C_m}{1 + (a_c(x) \eta k_v(T_s) \delta_c / k_c(x))} \quad (15)$$

Depending on the magnitude of the second term in the denominator of Eq. (15), the monolith reactor may be either in the kinetically controlled or mass transfer controlled regime. In the kinetically controlled regime, the fluid to solid mass transfer is much faster compared to the reaction rate and hence the fluid and solid phase concentrations are almost equal ($C_s \approx C_m$) and the second term in the denominator of Eq. (15) is much smaller than unity. When the reaction in the washcoat is much faster compared to the mass transfer from the fluid to the solid phase, which is usually the case after the monolith is ignited, the monolith is said to be in the mass transfer controlled regime and the concentration at the solid–fluid interface is close to zero ($C_s \simeq 0$) and the second term in the denominator of Eq. (15) is much greater than unity.

4. Light-off and cumulative emissions

We now explain briefly light-off and cumulative emissions. By ignition or light-off we mean that the steady-state bifurcation diagram of exit solid temperature $T_s(L)$ (or fluid phase exit conversion) versus the inlet fluid temperature $T_{f, \text{in}}$ is a S-shaped diagram with the ignition point in the feasible region. The shift from kinetically controlled regime to mass transfer controlled regime is characterized by ignition in the monolith.

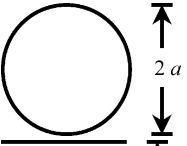

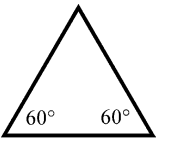
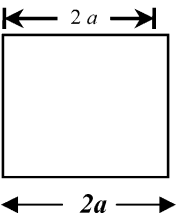
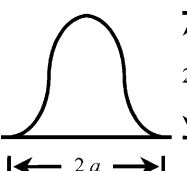
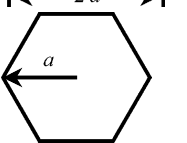
Catalytic converters used in automobiles are aimed at reducing the cumulative cold-start emissions. The cumulative emissions (in moles) for a single channel may be expressed as

$$E_{\text{cum}} = A_{\Omega} \bar{u} \int_0^t C_m(\tau', L) d\tau'$$

If the total mass flow rate is W (g/s), and the number of channels is N , the flow-rate through each channel is given by

$$A_{\Omega} \bar{u} = \frac{W}{N \rho_f}$$

Table 1
Effective diffusion length and asymptotic constants for some common channel geometries

Channel shape	R_Ω	$Nu(Sh)_{H_2,\infty}$	$Nu(Sh)_{H_1,\infty}$	$Nu(Sh)_{T,\infty}$	$f Re$	α_1
	$\frac{a}{2}$	4.364	4.364	3.656	16	0.81905
	a	8.235	8.235	7.541	24	0.91035
	$\frac{a}{2\sqrt{3}}$	1.893	3.111	2.497	13.33	0.7753
	$\frac{a}{2}$	3.089	3.608	2.977	14.23	0.8074
$\frac{a}{b} = 1$	$\frac{2a}{3}$	3.023	4.123	3.392	15.55	0.7891
$\frac{a}{b} = \frac{1}{2}$	$\frac{3a}{4}$	2.97	4.795	3.956	17.09	0.7695
$\frac{a}{b} = \frac{1}{3}$						
	$0.385a$	2.731	3.649	2.966	14.65	0.7872
	$\frac{\sqrt{3}}{4}a$	3.861	4.002	3.34	15.05	0.8156

Thus, the cumulative emissions from the start ($t = 0$) to time t , in grams may be expressed as

$$M_{\text{cum}} = NE_{\text{cum}}M_w = \left(\frac{W}{\rho_f}\right)M_w \int_0^t C_m(\tau', L) d\tau' \quad (16)$$

where M_w is the molecular weight of the reactant species. In Fig. 1, we replicate the graph produced by Oh and Cavendish [26] for cumulative emission of carbon monoxide for the standard converter. The plot shows the measured inlet and exit cumulative concentration as a function of time. By having a closer look of the figure, we could identify three regions. The first region (OA in Fig. 1) is the initial transient period, where the monolith is cold and is in the kinetically controlled regime. In this region, the surface concentration and the fluid phase concentrations are approximately the same, the reactant conversion is low (or emissions from the monolith are high). The third region (BC in Fig. 1) is where the monolith is ignited and is in the mass-transfer controlled

regime (which is also the steady state asymptote) where the surface concentration (over the ignited length) is much less than the fluid phase concentration and the exit reactant conversion is high (or low emissions). The second region (AB in Fig. 1) is the transient period during which an ignition front propagates through the monolith. During this period, the ignited length of the monolith increases with time attaining a steady-state value at B. It should be pointed out that when there is no ignition in the monolith these three regions cannot be differentiated. Fig. 2 shows a plot of the total cumulative emissions (in grams) for a typical set of parameters obtained by simulation of our model equations. [Unless otherwise mentioned, we always show the total cumulative emissions in the figures and not the cumulative emission from a single channel. In practice, the emissions per unit distance (g/mile) are of interest. This number can be obtained by dividing M_{cum} by the distance traveled, which is around 15 miles for $t = 30$ min.] Again, the plot shows three clearly defined regions. The difference between Figs. 1 and 2

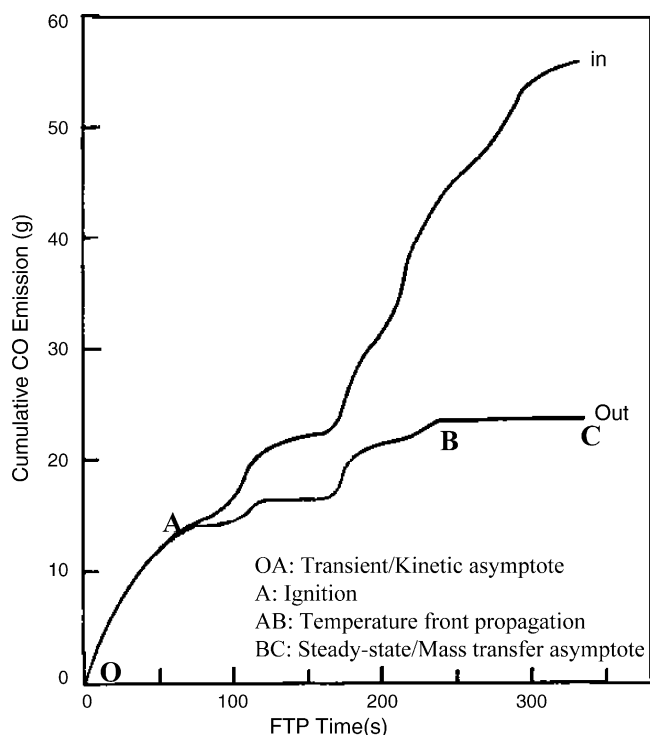


Fig. 1. Cumulative CO emission plot for the standard catalytic converter [26].

is observed in the region AB. In our simulations, we assume that the inlet concentration is constant with time whereas the work done of Oh and Cavendish accounts for inlet concentration varying with time. [It should be noted that we include

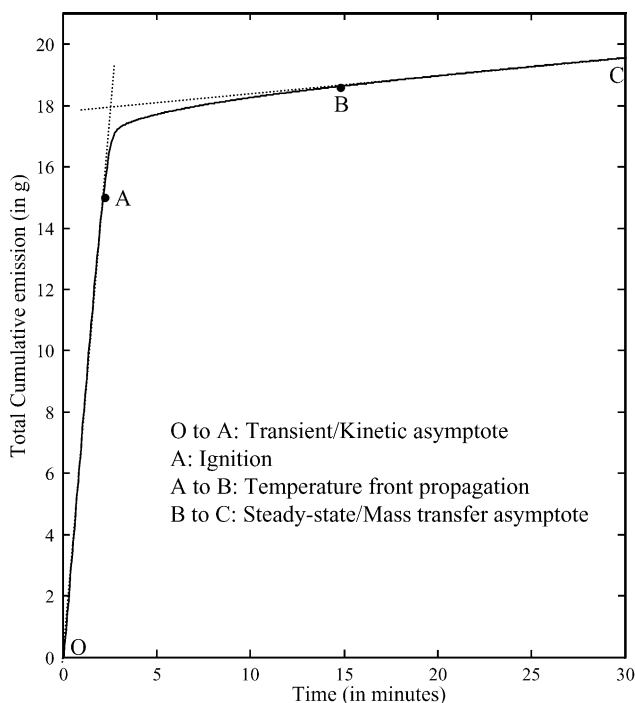


Fig. 2. Cumulative emission plot for typical parameter values (listed in Table 2).

the changes of inlet temperature with time like in the FTP cycle.] For the cumulative emissions to be lower, the transient time (from $t = 0$ to $t = t_A = t_{\text{ign}}$) should be lower and the steady-state conversion should be higher (or the slope of steady-state asymptote should be very small). Heat is transferred from the fluid to the solid until ignition after which the heat transfer is reversed. The occurrence of ignition in the monolith is represented by point A in Figs. 1 and 2. Once ignited, the temperature front travels upstream or downstream (or both) depending on the location where ignition first occurs.

In the transient asymptote (OA in Fig. 2), the exit conversion is very small and hence the exit concentration can be approximated by $C_{m,\text{exit}}(t) \approx C_{m,\text{in}}$ and the cumulative emissions in the transient asymptote ($t < t_{\text{ign}}$) is given by

$$M_{\text{cum}}(t) \approx \frac{W}{\rho_f} M_w C_{m,\text{in}} t \quad (17)$$

The steady-state exit conversion depends on the channel dimensions and the geometry of the channel. Once the monolith is ignited (BC in Fig. 2), the exit concentration is given by [24]

$$C_{m,\text{exit}} = C_{m,\text{in}} \alpha_1 \exp\left(-\frac{Sh_{T,\infty} L_{\text{ign}} D_m}{4R_\Omega^2 \bar{u}}\right) \quad (18)$$

where α_1 is the Fourier weight and is equal to 0.819 for a fully developed laminar flow in a circular duct, $Sh_{T,\infty}$ is the asymptotic Sherwood number for constant wall concentration case and L_{ign} is the ignited length of the monolith (or the length of the monolith in the mass transfer controlled regime). As can be seen, after ignition, in the mass transfer controlled regime, the exit concentration depends only on the channel geometry ($Sh_{T,\infty}$), channel dimensions (R_Ω and L), and the effective channel residence time (L_{ign}/\bar{u}) and not on the reaction parameters. For the case of front-end ignition, we could get approximate analytical expression for the exit conversion and is presented in Sections 6 and 7.

From the above discussion, it is clear that the minimization of the cumulative cold-start emissions requires a detailed understanding of the ignition or light-off behavior, front propagation and the mass transfer controlled (ignited) regime in the monolith. Each of these depends on the activity profile, as well as other design and operating parameters. In the following sections, we consider these in more detail.

5. Light-off with nonuniform catalyst loading

In this and the next section, we discuss the various design criteria that are needed for optimal design of the monolith to reduce the transient emissions. First, we discuss the light-off criterion which has been obtained in our previous work [22].

This analytical light-off criterion when satisfied will favor ignition in the monolith at the inlet fluid temperature $T_{f,in}$. The light-off criterion for the general case of nonuniform catalyst loading is

$$\left(\frac{g(Pe_h)\omega(\varphi)}{f(\varphi)} \frac{(-\Delta H_R)C_{m,in}E\delta_c Lk_v(T_{f,in})}{\rho_f c_{pf} R_\Omega \bar{u} R_g T_{f,in}^2} + \frac{4e\max[a_c(x)]}{f(\varphi_{\max})} \frac{(-\Delta H_R)C_{m,in}E\delta_c R_\Omega k_v(T_{f,in})}{Nu_{H1,\infty} R_g T_{f,in}^2 k_f} \right) > 1 \quad (19)$$

where $\varphi = \delta_c \sqrt{k_v(T_{f,in})/D_e}$ is the washcoat Thiele modulus at the inlet fluid temperature, $\varphi_{\max} = \delta_c \sqrt{\max[a_c(x)]k_v(T_{f,in})/D_e}$ and $Pe_h = \bar{u} L \rho_f c_{pf} R_\Omega / (k_w \delta_w)$ is the axial heat Peclet number. The functions $g(Pe_h)$, $f(z)$ and $\omega(\varphi)$ are given as

$$g(Pe_h) = \frac{1}{(\sigma_\theta^2) \sigma_\theta^2 / (1 - \sigma_\theta^2)}, \quad \sigma_\theta^2 = \frac{2}{Pe_h} - \frac{2}{Pe_h^2} (1 - e^{-Pe_h})$$

$$f(z) = \begin{cases} 1 & z < 0.5 \\ 2z & z > 0.5 \end{cases}$$

and

$$\omega(\varphi) = \begin{cases} 1 & \varphi < 0.5 \\ \frac{1}{L} \int_0^L \sqrt{a_c(x)} dx & \varphi > 0.5 \end{cases}$$

In the above expressions, $g(Pe_h)$ describes the influence of solid conduction and the functions $f(\varphi)$ and $\omega(\varphi)$ represents the influence of washcoat diffusion in the catalyst. The first term in the ignition criterion (Eq. (19)) represents ignition at the reactor scale and the second term in the criterion represents local ignition. Depending on the magnitude of the terms, we could determine the nature of ignition in the monolith. If the first term exceeds unity and the second term is negligible compared to unity we have a back-end ignition. For back-end ignition, the monolith ignites first near the exit of the reactor and the temperature front propagates upstream with the help of solid conduction. When the second term exceeds unity (with the first term negligible compared to the second term), then the ignition occurs at the location where the catalyst distribution function $a_c(x)$ is maximum. In this case, the temperature front will propagate both upstream (with the help of solid conduction) and downstream (with the help of solid conduction and convection in the fluid phase). If the maximum of $a_c(x)$ occurs at $x = 0$, that is at the inlet, then we have a front-end ignition. [If the catalyst loading is uniform over a finite length $0 < z < z^*$ then the ignition occurs at the front-end of this section.] When the ignition criterion is barely satisfied and the magnitude of both the terms is less than unity, it is always a back-end ignition. It should be noted that there is a minimum value of $k_v(T_{f,in})$ below which there is no ignition in the converter.

It has been shown previously [17] that the transient times are lower for the case of front-end ignition, followed by middle and back-end ignition. Hence, it is advantageous to place more amount of the catalyst near the inlet to favor front-end ignition thereby reducing the transient time. From the ignition criterion, we could distribute the catalyst such that the function $a_c(x)$ is high close to the inlet. The criteria that should be satisfied for a front-end ignition can be written as

$$\frac{4e\max[a_c(x)]}{f(\delta_c \sqrt{\max[a_c(x)]k_v(T_{f,in})/D_e})} \frac{(-\Delta H_R)C_{m,in}E\delta_c R_\Omega k_v(T_{f,in})}{Nu_{H1,\infty} R_g T_{f,in}^2 k_f} > 1 \quad (20)$$

with $a_c(x)$ having a maximum value close to the inlet. Note that the solid conduction does not appear in the above criterion and it has been shown [22] that front-end ignition is independent of solid conduction. Also, higher values of the term on the LHS of Eq. (20) lead to lower transient times [22].

As can be seen from the ignition criterion, the washcoat diffusion has a profound influence. For very low values of the washcoat thickness, the function $f(\varphi_{\max})$ equals unity and increasing the washcoat thickness decreases the inlet temperature required for ignition and also the transient time. But once washcoat thickness increases beyond a critical value, strong washcoat diffusional limitations exist and the temperature required for ignition does not decrease any more and the transient time remains the same. In addition, higher the value of $\max[a_c(x)]$, lower the value of the inlet fluid temperature required for ignition. To make effective use of all the precious metal in the washcoat, the optimum washcoat thickness that should be used is the maximum value at washcoat diffusional limitations do not exist. This is given by

$$\varphi_{\max} = \delta_c \sqrt{\frac{\max[a_c(x)]k_v(T_{f,in})}{D_e}} = \frac{1}{2} \quad (21)$$

When the above criterion for washcoat thickness (or metal loading) is satisfied, the criterion for front-end ignition can be reduced to

$$4e\max[a_c(x)] \frac{(-\Delta H_R)C_{m,in}E\delta_c R_\Omega k_v(T_{f,in})}{Nu_{H1,\infty} R_g T_{f,in}^2 k_f} > 1 \quad (22)$$

as the function $f(\varphi_{\max})$ equals unity for values of $\varphi_{\max} \leq 1/2$.

Our focus till now was to reduce the transient time so that the cumulative emissions can be reduced. The above two criteria given by Eqs. (20) and (21) favor front-end ignition and reduce the transient time considerably. The steady-state conversion is also as important as the transient time because for converters operating for times much longer than the transient times, the cumulative emissions are determined by the steady-state concentrations. After ignition in the

monolith we require the entire monolith to be in the mass transfer controlled regime (with the ignited length of the monolith L_{ign} is as large as possible) so that the exit concentration will reach the minimum possible value as seen in Eq. (18). As mentioned earlier, in the mass transfer controlled regime the reaction rates are much faster compared to the mass transfer rates from the fluid to the solid phase. This defines a minimum catalyst loading required (so that the reaction rate after ignition is much higher than the mass transfer rate) and is given by the second term in the denominator of Eq. (15) being much greater than unity, i.e.

$$\frac{a_c(x)\eta k_v(T_{s,ss})\delta_c}{k_c(x)} \gg 1 \quad (23)$$

Here, $T_{s,ss}$ represents the solid temperature after ignition which is usually $T_{f,in} + \Delta T_{ad}$ (at steady-state). After ignition, the solid temperature is high and hence the washcoat Thiele modulus ($\delta_c \sqrt{k_v(T_{s,ss})a_c(x)/D_e}$) will be large and the effectiveness factor can be approximated by

$$\eta = \frac{1}{(\delta_c \sqrt{k_v(T_{s,ss})a_c(x)/D_e})} \quad (24)$$

The mass transfer coefficient $k_c(x)$ can be approximated by the asymptotic value ($Sh_{H_1,\infty} D_m / 4R_\Omega$) and the catalyst distribution function $a_c(x)$ can be replaced by its minimum value $\min[a_c(x)]$. With these approximations the criterion for mass transfer controlled (or the lower bound on catalyst loading) can be written as

$$\frac{4R_\Omega}{Sh_{H_1,\infty} D_m} \sqrt{\min[a_c(x)] D_e k_v(T_{s,ss})} \gg 1 \quad \text{or} \quad \frac{4R_\Omega}{Sh_{H_1,\infty} D_m} \sqrt{\min[a_c(x)] D_e k_v(T_{s,ss})} > 10 \quad (25)$$

When the above criterion is satisfied, the entire monolith is in the mass transfer controlled regime and the maximum possible conversion ($L_{\text{ign}} = L$ in Eq. (18)) is obtained. [The value of 10 used in the above criterion (Eq. (25)) is arbitrary and any value much greater than unity should suffice.] The length of the reactor to achieve the required conversion can be obtained from Eq. (18).

The above criteria given by Eqs. (20), (21) and (25) summarize the important design criteria which aim to reduce the cumulative emissions. These criteria can be analyzed further by expanding the reaction rate constant in terms of the temperature. The rate constant can be expressed as

$$k_v(T) = k_{v0} \exp\left(\frac{E}{R_g T_{f,in}} - \frac{E}{R_g T}\right)$$

where k_{v0} is the reaction rate constant at temperature $T_{f,in}$. The above criteria can be rewritten as

$$\left[4e \frac{(-\Delta H_R) C_{m,in} E \delta_c R_\Omega}{Nu_{H_1,\infty} R_g T_{f,in}^2 k_f} \right] \max[a_c(x)] k_{v0} > 1 \quad (26)$$

$$\left[\frac{1}{D_e} \right] \max[a_c(x)] k_{v0} \delta_c^2 = \frac{1}{4} \quad (27)$$

$$\left[\frac{16R_\Omega^2}{Sh_{H_1,\infty}^2 D_m^2} D_e \exp\left(\frac{E}{R_g T_{f,in}} - \frac{E}{R_g T_{s,ss}}\right) \right] \min[a_c(x)] k_{v0} > 100 \quad (28)$$

The design parameters are usually the precious metal loading (k_{v0}), the catalyst distribution along the channel length ($a_c(x)$) and the washcoat thickness (δ_c). The optimum washcoat thickness can be easily obtained from Eq. (27) and Eq. (26) represents the criterion for front-end ignition (to reduce transient time) and Eq. (28) represents the criterion for mass transfer control (to obtain higher conversion). The front-end ignition criterion, when satisfied, reduces the transient time and the criterion for mass transfer control, when satisfied, gives the maximum possible steady-state conversion and does not affect the transient time significantly. It is easily seen that for typical values of reaction parameters, Eq. (28) is a more stringent criterion than Eq. (26).

If the metal loading (k_{v0}) is such that Eq. (28) can be satisfied easily for uniform catalyst distribution, then we could redistribute so that the LHS of Eq. (26) is higher and hence the transient time will be lower. In this case, the value of $\min[a_c(x)]$ could be found such that Eq. (28) is barely satisfied and we could correspondingly find $\max[a_c(x)]$ which will reduce the transient time further. If the metal loading is such that Eq. (28) cannot be satisfied for uniform catalyst distribution (and Eq. (26) is satisfied) then instead of forcing a front-end ignition by redistributing the catalyst, it is better to have uniform catalyst distribution. This is because redistributing the catalyst will reduce the quantity on LHS of Eq. (28) and hence the steady-state conversion will be lower. [Note that cumulative emissions also depend on the time duration the converter will be operated. We assume that the transient time is small compared to the total time and hence steady-state conversion will also have a considerable impact on the cumulative emissions. If the total time duration of operation is small, then in this case also, it will be better to have front-end ignition to reduce transient time though the steady-state conversion may not be high.] In the extreme case where the metal loading does not satisfy Eqs. (26) and (28) for uniform catalyst distribution, both the transient time will be high and steady-state conversion will be low. We could redistribute the catalyst to favor front-end ignition thereby reducing the transient time. But the converter will not reach the mass transfer controlled regime

and hence the steady-state conversion will still be low. The above analysis could be summarized as:

- Uniform catalyst loading best for

$$k_{v0} \in \left[\left(\frac{Nu_{H1,\infty} R_g T_{f,in}^2 k_f}{4e(-\Delta H_R) C_{m,in} E \delta_c R_\Omega} \right), \left(\frac{100 Sh_{H1,\infty}^2 D_m^2}{16 R_\Omega^2 D_e} \exp \left(\frac{E}{R_g T_{s,ign}} - \frac{E}{R_g T_{f,in}} \right) \right) \right]$$

- Nonuniform catalyst loading best for

$$k_{v0} \notin \left[\left(\frac{Nu_{H1,\infty} R_g T_{f,in}^2 k_f}{4e(-\Delta H_R) C_{m,in} E \delta_c R_\Omega} \right), \left(\frac{100 Sh_{H1,\infty}^2 D_m^2}{16 R_\Omega^2 D_e} \exp \left(\frac{E}{R_g T_{s,ign}} - \frac{E}{R_g T_{f,in}} \right) \right) \right]$$

- Optimum washcoat thickness

$$\left[\frac{1}{D_e} \right] \max[a_c(x)] k_{v0} \delta_{c,opt}^2 = \frac{1}{4}$$

The value 10 used in the criterion for mass transfer c-controlled is arbitrary and smaller this value, smaller is the range of k_{v0} values for which uniform catalyst distribution is better. It should be noted that the above analysis is performed assuming that the transfer coefficients are constant and can be easily extended to the case where transfer coefficients vary with position. With varying transfer coefficients, it will become harder to obtain front-end ignition because of the Nusselt number appearing in the denominator of the front-end ignition criterion. Also, it becomes difficult to satisfy the mass transfer controlled criterion with varying transfer coefficients. When the transfer coefficients are large (than the constant asymptotic value) near the inlet, the mass transfer rates will be high and hence the reaction rates after ignition should be much higher so that the inlet of the converter is in the mass transfer controlled regime. Hence, near the inlet (where the transfer coefficients are high) a nonuniform catalyst distribution with more catalyst near the inlet would actually satisfy the mass transfer controlled criterion easily compared to uniform catalyst loading. The converse is true in the fully developed region (when the transfer coefficients are constant) i.e., uniform catalyst loading would satisfy the mass transfer controlled criterion easily compared to non-uniform catalyst loading.

6. Ignition and temperature front propagation times

We have illustrated in the previous section, the effect of nonuniform catalyst distribution on the cumulative emissions. By distributing the catalyst appropriately along the length of the channel, it is possible to favor front-end ignition. The time required to reach the steady state

asymptote can be split into the ignition time and the propagation time (the times corresponding to OA and AB in Fig. 2, respectively). This ignition time consists of the heat-up time and the time required for the solid to reach the ignition temperature (from the inlet fluid temperature). The heat-up time is the time required for the monolith to reach the inlet fluid temperature from its initial temperature. This process is mainly controlled by heat transfer from the fluid to the solid (and depends on the channel geometry) as the heat generated by the reaction is usually negligible during this period. This heat-up time depends mainly on the difference between the inlet fluid temperature and the initial solid temperature. The ignition time of the monolith depends more on the nature of ignition (front-end, middle or back-end), and hence on the catalyst loading and the inlet fluid temperature. It has already been shown [17] that front-end ignition leads to the shortest transient time while back-end ignition has the longest transient time. For the case of front-end ignition, low solid conduction and constant inlet temperature, the ignition time (t_{ign}) can be obtained analytically by integrating Eq. (4). At the inlet, $T_f = T_{f,in}(t)$ and the transient time can be obtained by integrating the following equation until the solid temperature reaches the ignition temperature ($T_{s,ign}$).

$$\frac{dT_s}{dt} = \frac{1}{\delta_w \rho_w c_{pw}} \left[(-\Delta H_R) a_c(0) k_v(T_s) C_{s,in} \delta_c \eta - \frac{k_f Nu_{H1,\infty}}{4 R_\Omega} (T_s - T_{f,in}(t)) \right] \quad (29)$$

where

$$\eta = \frac{\tanh(\delta_c \sqrt{k_v(T_s) a_c(0) / D_e})}{(\delta_c \sqrt{k_v(T_s) a_c(0) / D_e})}$$

$$C_{s,in} = \frac{C_{m,in}}{1 + (4 a_c(0) R_\Omega \eta k_v(T_s) \delta_c / Sh_{H1,\infty} D_m)}$$

The ignition temperature is given by

$$T_{s,ign} \simeq \frac{R_g T_{f,in}^2}{E} \ln \left[\frac{k_f Nu_{H1,\infty} R_g T_{f,in}^2}{4 C_{m,in} E \delta_c R_\Omega (-\Delta H_R) a_c(0) k_v(T_{f,in})} \right] + T_{f,in} \quad (30)$$

where $T_{f,in}$ is the steady-state value of the inlet fluid temperature (in this case 600 K). The above expression is obtained by differentiating the steady-state version of Eq. (29) with respect to T_s and equating it to zero. We also make use of the assumption of positive exponential approximation and negligible reactant consumption in obtaining the above result. In the above equations, $a_c(0)$ represents the value of the catalyst distribution function at $x = 0$. [Note: For the sake of simplicity, we approximated the heat and mass transfer coefficients near the inlet by the asymptotic value.] From the above equation for $T_{s,ign}$, the effect of the reaction parameters and the catalyst distribution on the ignition temperature is easily seen. For the special case of constant

inlet fluid temperature, Eq. (29) can be rewritten as

$$t_{\text{ign}} = \int_{T_{s0}}^{T_{s,\text{ign}}} \frac{\delta_w \rho_w c_{pw} dT_s}{(-\Delta H_R) a_c(0) k_v(T_s) C_{s,\text{in}} \delta_c \eta - (k_f Nu_{H1,\infty} / 4R_\Omega)(T_s - T_{f,\text{in}})} \quad (31)$$

to obtain the ignition time.

Once the monolith is ignited and reaches the ignition temperature, the temperature front propagates in the flow direction and reaches the exit of the monolith. The propagation time (t_{prop}) can be estimated analytically for the case of the pseudohomogeneous model (where the temperature and concentration difference between the solid and the fluid phase are negligible). [The time taken by the reactor to reach a specified temperature at the exit after the inlet reaches the specified temperature is called the propagation time.] The energy balance equation for the pseudohomogeneous model for low solid conduction can be written as

$$\delta_w \rho_w c_{pw} \frac{\partial T}{\partial t} + \bar{u} \rho_f c_{pf} R_\Omega \frac{\partial T}{\partial x} = (-\Delta H_R) a_c(x) R_v(C, T) \delta_c \eta \quad (32)$$

This is a nonlinear hyperbolic equation. The speed of the temperature front can be obtained from the characteristic equation of (32) and is given by

$$\frac{dx}{dt} = \frac{\bar{u} \rho_f c_{pf} R_\Omega}{\rho_w c_{pw} \delta_w}$$

and the time required for the temperature front to propagate downstream to reach the exit of the monolith can be expressed as

$$t_{\text{prop}} = \frac{L \rho_w c_{pw} \delta_w}{\bar{u} \rho_f c_{pf} R_\Omega} \quad (33)$$

or in other terms

$$\tau_{\text{prop}} = \frac{t_{\text{prop}} \bar{u}}{L} \frac{\rho_f c_{pf} R_\Omega}{\rho_w c_{pw} \delta_w} = 1 \quad (34)$$

where τ_{prop} is the dimensionless propagation time. Though this result is obtained for the pseudohomogeneous model, it is good even for the two-phase model as long as the transverse Peclet number is small. The transverse Peclet number, $P = R_\Omega^2 \bar{u} / LD_m$, is defined as the ratio of the transverse diffusion time to the convection (residence) time. For $P \rightarrow 0$, the two-phase model reduces to the pseudohomogeneous model. The typical P values used in catalytic converters are around 0.1–0.3 and for values of $P \ll 1$, the propagation time can be approximated by Eqs. (33) or (34). The results will be validated by numerical simulations in Section 8. Hence, the total time taken to reach the mass transfer controlled regime is the sum of the transient time given by Eq. (29) and the propagation time given by Eq. (33). For minimizing cumulative emissions this total

time has to be minimized. [Note: Eq. (33) gives the propagation time only for the case of front-end ignition. It is hard to obtain analytical expressions for the propagation time for the case of back-end ignition. Nevertheless, it is clearly seen that the propagation time for front-end ignition is much smaller compared to the propagation time in the case of back-end ignition. Numerical simulations in the Section 8 will illustrate this in a little more detail.]

7. Estimation of cumulative emissions

In this section, we shall obtain an estimate of the cumulative cold-start emissions for the case of front-end ignition using the results obtained in the previous sections. In the transient/kinetic asymptote (OA in Fig. 2), the cumulative emissions is given by Eq. (17) and is written as

$$C_{m,\text{exit,OA}} \simeq C_{m,\text{in}}, \quad t < t_{\text{ign}} \quad (35)$$

where t_{ign} is the time taken for ignition to occur in the monolith.

After ignition (at front-end), the temperature front propagates and the ignited length keeps increasing. During this period (A–B in Fig. 2), if the ignited length of the monolith is in the mass transfer controlled regime, then the exit concentration can be written as

$$C_{m,\text{exit,AB}} \simeq C_{m,\text{in}} \alpha_1 \exp \left(-\frac{Sh_{T,\infty} D_m}{4R_\Omega \delta_w} \frac{\rho_f c_{pf}}{\rho_w c_{pw}} (t - t_{\text{ign}}) \right), \quad t_{\text{ign}} < t < t_{ss} \quad (36)$$

where $t_{ss} = t_{\text{ign}} + t_{\text{prop}}$. The above expression for the exit concentration is obtained by substituting for the ignited length from Eq. (33) into Eq. (18). After the temperature front has completely propagated through the channel, the exit concentration is given by (assuming that the entire monolith is in the mass transfer controlled regime) Eq. (18) and is written as

$$C_{m,\text{exit,BC}} \simeq C_{m,\text{in}} \alpha_1 \exp \left(-\frac{Sh_{T,\infty} LD_m}{4R_\Omega^2 \bar{u}} \right), \quad t_{ss} < t < t_{\text{final}} \quad (37)$$

where t_{final} is the final time. The cumulative cold-start emissions (in grams) can now be expressed as

$$M_{\text{cum,total}} \simeq \left(\frac{W}{\rho_f} \right) M_w \left[\int_0^{t_{\text{ign}}} C_{m,\text{exit,OA}} dt + \int_{t_{\text{ign}}}^{t_{ss}} C_{m,\text{exit,AB}} dt + \int_{t_{ss}}^{t_{\text{final}}} C_{m,\text{exit,BC}} dt \right] \quad (38)$$

Substituting Eqs. (35) to (37) in the above expression, the total emissions can be written as

$$\begin{aligned}
 M_{\text{cum,total}} &\simeq \left(\frac{W}{\rho_f}\right) M_w \left[C_{\text{m,ign}} t_{\text{ign}} + \int_{t_{\text{ign}}}^{t_{\text{ss}}} C_{\text{m,ign}} \alpha_1 \right. \\
 &\quad \times \exp\left(-\frac{Sh_{T,\infty} D_m}{4R_{\Omega} \delta_w} \frac{\rho_f c_{\text{pf}}}{\rho_w c_{\text{pw}}}(t - t_{\text{ign}})\right) dt \\
 &\quad \left. + C_{\text{m,ign}} \alpha_1 \exp\left(-\frac{Sh_{T,\infty} L D_m}{4R_{\Omega}^2 \bar{u}}\right) (t_{\text{final}} - t_{\text{ss}}) \right] \\
 &= \left(\frac{W}{\rho_f}\right) M_w \left[C_{\text{m,ign}} t_{\text{ign}} + \frac{4R_{\Omega} \delta_w \rho_w c_{\text{pw}} C_{\text{m,ign}} \alpha_1}{Sh_{T,\infty} D_m \rho_f c_{\text{pf}}} \right. \\
 &\quad \times \left\{ 1 - \exp\left(-\frac{Sh_{T,\infty} L D_m}{4R_{\Omega}^2 \bar{u}}\right) \right\} \\
 &\quad \left. + C_{\text{m,ign}} \alpha_1 \exp\left(-\frac{Sh_{T,\infty} L D_m}{4R_{\Omega}^2 \bar{u}}\right) (t_{\text{final}} - t_{\text{ss}}) \right\} \quad (39)
 \end{aligned}$$

As mentioned earlier, t_{ign} is obtained by integrating Eq. (29) until the solid reaches the ignition temperature ($T_{\text{s,ign}}$, given by Eq. (30)) from the initial solid temperature (T_{s0}). From the above expression, we could clearly see the effect of various design parameters on the cumulative emissions. Only the ignition time (t_{ign}) depends on the reaction parameters and the steady-state concentration and the propagation time is nearly independent of the reaction parameters. [Remark: Eq. (39) is valid only for a front-end ignition and assuming that after ignition, the monolith reaches the mass-transfer controlled regime i.e., Eq. (25) is satisfied for all values of 'x'.]

In the above analysis, it is assumed that once the ignition temperature is reached, the time taken to reach the mass transfer controlled regime is negligible. We can relax this assumption and could calculate the ignition time by integrating Eq. (29) until the solid temperature reaches the transition temperature ($T_{\text{s,trans}}$). The transition temperature $T_{\text{s,trans}}$ (the temperature at which the mass transfer resistance and the kinetic resistance becomes equal, i.e., the two terms in the denominator of Eq. (15) are equal) is given by the root of the equation

$$\begin{aligned}
 &\left(\delta_c \sqrt{\frac{k_v(T_s) a_c(0)}{D_e}} \right) \\
 &= \frac{4a_c(0) R_{\Omega} k_v(T_s) \delta_c}{Sh_{H_1,\infty} D_m} \tanh\left(\delta_c \sqrt{\frac{k_v(T_s) a_c(0)}{D_e}} \right) \quad (40)
 \end{aligned}$$

For the parameter values given in Table 2, the difference between the ignition and the transition temperature is around 100–150 K depending on the activity profile. Using the transition temperature to find the ignition time will be a more accurate estimation of the total cumulative emissions.

Table 2

Standard set of parameter values used for simulations

\bar{u}	5 m/s	k_f	0.0472 W/m K
R_{Ω}	0.5 mm	k_w	0.8304 W/m K
δ_s	150 μm	A_f	$9.6 \times 10^9 \text{ s}^{-1}$
δ_c	25 μm	$(-\Delta H_R)$	$1.6 \times 10^6 \text{ J/mol}$
ρ_f	0.58 kg/m^3	E/R_g	10800 K
c_{pf}	$1.089 \times 10^3 \text{ J/kg K}$	D_e	$8 \times 10^{-6} \text{ m}^2/\text{s}$
ρ_w	2500 kg/m^3	D_m	$8.82 \times 10^{-5} \text{ m}^2/\text{s}$
c_{pw}	$1.38 \times 10^3 \text{ J/kg K}$	$C_{\text{m,ign}}$	0.12 mol/m^3
L	0.1 m	W	13.6 g/s
M_w	44		

8. Numerical simulations

In this section, we present some numerical simulations that illustrate the important points discussed in the previous section. A typical FTP-75 cycle is approximated by an inlet fluid temperature profile with time as shown in Fig. 3. The inlet fluid temperature keeps increasing from ambient temperature (300 K) to 600 K at the rate of approximately 4 K/s. After 80 s, the inlet fluid temperature remains constant at 600 K. For the rest of the work, we shall use this inlet fluid temperature profile unless mentioned otherwise. [For comparison purposes, we shall also consider the case in which $T_{\text{f,in}}(t)$ is a step function (300–600 K at $t = 0$).] For the simulations, propane oxidation is considered. Unless otherwise stated in the figure, the kinetic parameters [27] along with the other standard set of parameter values as shown in Table 2 are used for the simulations. The

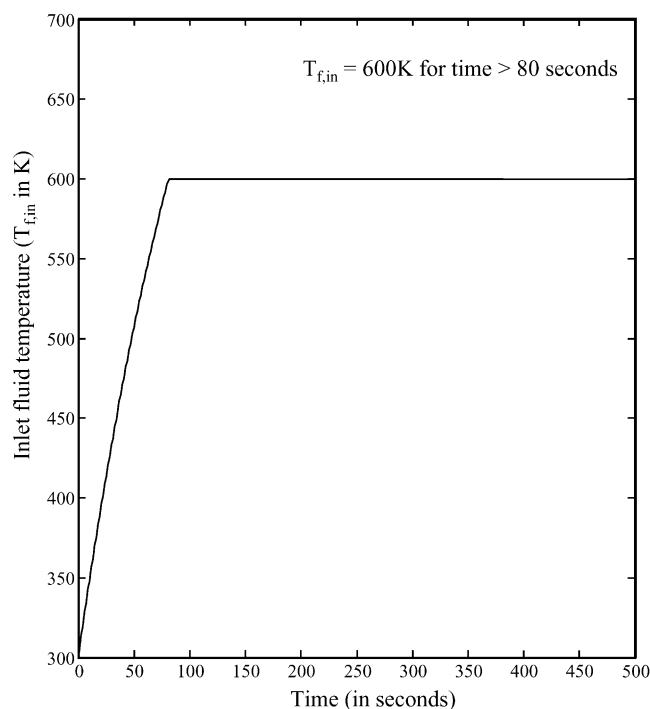


Fig. 3. Variation of inlet fluid temperature with time (approximation of FTP-75 cycle).

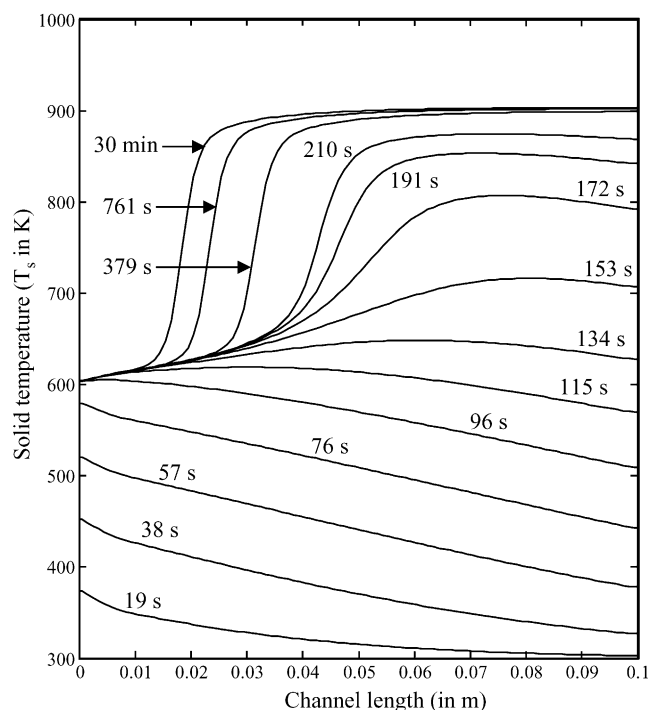


Fig. 4. Solid temperature profiles along the channel length at different time instants for typical parameter values and uniform catalyst distribution.

simulations are done for a total time of 30 min and the cumulative emissions obtained at $t = 30$ min are compared.

For the standard set of parameters listed in Table 2, a uniform catalyst distribution favors a back-end ignition and the cumulative emissions plot for this case was already shown in Fig. 2. The solid temperature profiles at different time instants are shown in Fig. 4. Unless mentioned otherwise, the initial solid temperature used for the simulations is 300 K. The cold monolith gets heated by the incoming fluid and once the monolith is ignited, the heat transfer is reversed from the solid to the fluid phase. It can be seen from the figure that it takes approximately 115 s for the monolith to get heated to the fluid temperature after which ignition occurs close to the exit of the reactor and the temperature front travels upstream. Since the temperature front travels against the flow direction, the speed of the front is low and is aided only by conduction in the solid phase. After 30 min, approximately 80% of the channel length is ignited and the exit conversion is approximately 99.24%. [Note that after ignition, the second term in the denominator of Eq. (15) is around 3.6 for set of parameters used.] Also, the value of k_{v0} falls in the region where front-end ignition is not favored and the criterion for mass transfer controlled operation is not satisfied. Hence, as discussed earlier, nonuniform catalyst distribution should improve the performance of the converter. The same set of parameters is used for the simulation of a two-zone catalyst distribution with more catalyst near the inlet. The two zones are chosen such that front-end ignition is favored. The chosen catalyst

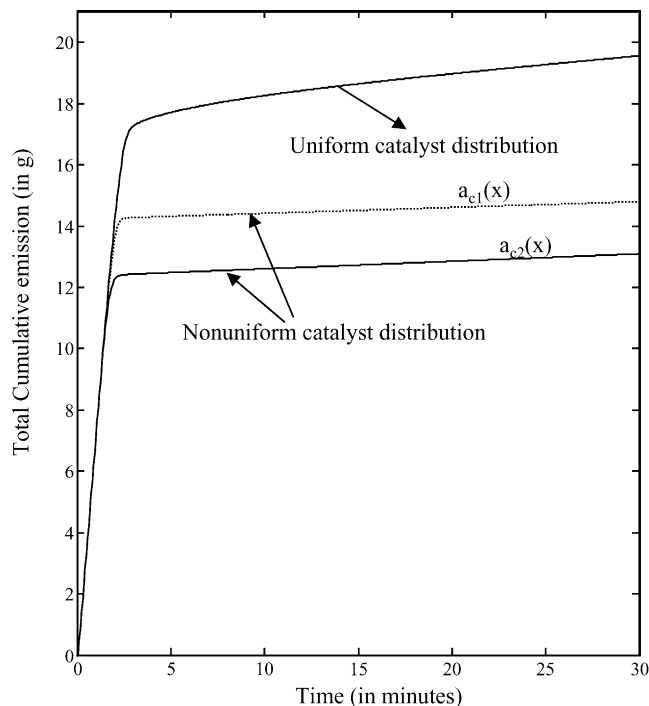


Fig. 5. Cumulative emissions plot for three different catalyst distribution for parameter values listed in Table 2.

distribution are given by

$$a_c(x) = a_{c1}(x) = \begin{cases} 3 & x < 0.01 \\ \frac{7}{9} & x > 0.01 \end{cases}$$

$$a_c(x) = a_{c2}(x) = \begin{cases} 5 & x < 0.01 \\ \frac{5}{9} & x > 0.01 \end{cases}$$

The cumulative emissions plot for these distributions are shown in Fig. 5. For comparison purposes we also show the cumulative emissions for the case of uniform catalyst distribution. As can be seen, the cumulative emissions for nonuniform catalyst loading is significantly less compared to the case of uniform catalyst distribution (more than 30%). It is also seen that for nonuniform catalyst loading the ignition occurs around 40–60 s earlier than the uniform catalyst distribution case. Another important observation is that the propagation time for the case of uniform catalyst loading where a back-end ignition occurs is much larger compared to the case of front-end ignition (with catalyst distributions $a_{c1}(x)$ and $a_{c2}(x)$). In Figs. 6 and 7, we show the temperature profiles at different time instants for the case of nonuniform catalyst distribution $a_{c1}(x)$ and $a_{c2}(x)$, respectively. The monolith ignites close to the inlet and the temperature front travels downstream. As can be seen, the temperature front travels much faster (because of convection in the fluid phase and conduction in the solid phase) and reaches steady-state (where the entire monolith is ignited) much early as compared to the case of uniform catalyst distribution. The steady-state exit conversion for this case is around 99.74 and 99.67% for the catalyst

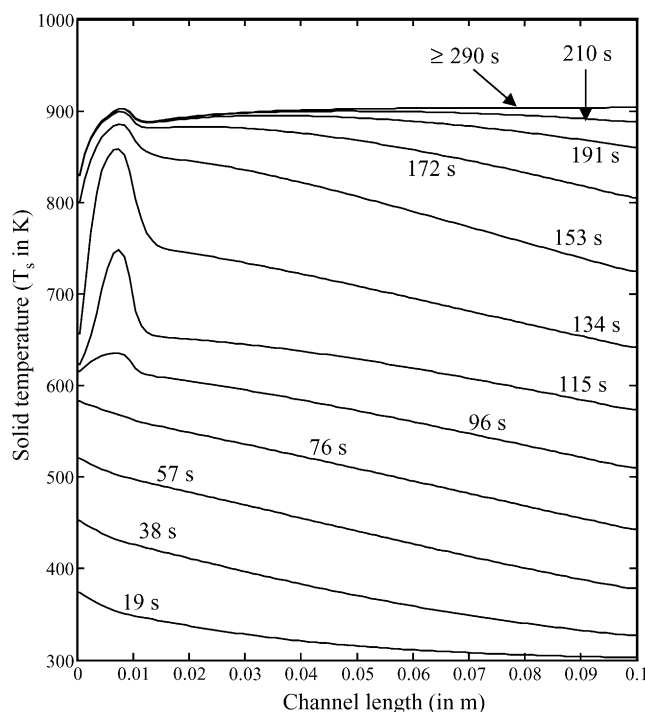


Fig. 6. Solid temperature profiles along the channel length at different time instants for typical parameter values and catalyst distribution $a_{c1}(x)$.

distribution $a_{c1}(x)$ and $a_{c2}(x)$, respectively. The transient time is lower for the catalyst distribution $a_{c2}(x)$ than $a_{c1}(x)$ because of more amount of catalyst near the inlet, but it has the disadvantage of lower conversion because of less amount

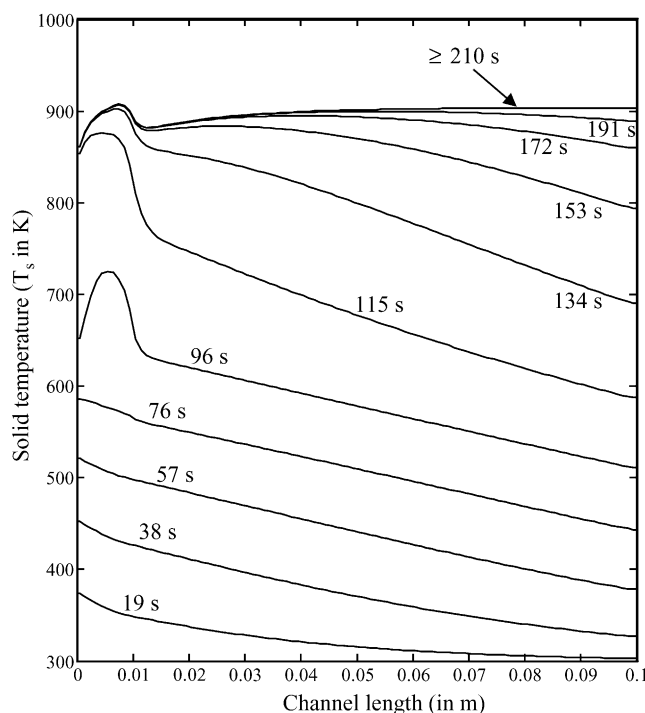


Fig. 7. Solid temperature profiles along the channel length at different time instants for typical parameter values and catalyst distribution $a_{c2}(x)$.

of catalyst (which makes it difficult to attain the mass transfer controlled regime) in the rest of the channel section. [Note: For the case of uniform catalyst distribution we had a back-end ignition with 80% of the channel length ignited. But if the parameter values are such that uniform catalyst distribution favors a back-end ignition with only 40–50% of the channel length ignited, then the cumulative emissions would be much higher and a nonuniform catalyst distribution for this case would yield 70–80% less emissions.]

For higher values of the catalyst loading (k_{v0}), which satisfies the front-ignition criterion for uniform catalyst loading and does not satisfy the criterion for mass transfer control, nonuniform catalyst loading may not improve the performance of the converter. This is because redistributing the catalyst to reduce the transient time further, might decrease the steady-state conversion. In the section of the catalyst where the amount of catalyst is low, the reaction rates after ignition will be comparatively low (the second term in the denominator of Eq. (15) will be small compared to its value in the zone where the amount of catalyst is high) and hence this section of the monolith may be far from the mass transfer controlled regime. Hence, for these values of k_{v0} uniform catalyst distribution is better. As mentioned earlier, if the total time is not high compared to transient time, then even in this range of k_{v0} , nonuniform catalyst loading is better. For much higher values of k_{v0} which satisfies the criterion for both front-end ignition and mass transfer control (for uniform catalyst loading), we could find a value of $\min[a_c(x)]$ such that the criterion for mass transfer control is barely satisfied and redistribute this excess catalyst such that there is more catalyst near the front. This would make sure that the entire monolith is still in the mass transfer controlled regime to achieve good steady-state conversion and would also reduce the transient time further because of more catalyst near the inlet. We do not show plots illustrating this, as it can be seen intuitively.

The influence of the catalyst loading (k_{v0}) (or the frequency factor) on the cumulative emissions (and the transient time) can be seen in Fig. 8. The cumulative emissions after 30 min is shown as a function of the catalyst loading for three different catalyst distributions. For very low catalyst loading there is no ignition in the monolith for all three catalyst distribution. As the catalyst loading increases for uniform distribution, back-end is first favored and then as A_r increases further front-end ignition is favored. The cumulative emissions keeps decreasing as the transient time decreases as we increase A_r . Similar behavior is observed for the two-zone distribution. One important observation is that for the two-zone distribution, the minimum value of A_r required for ignition is smaller and front-end ignition is favored easily, as expected. A second important observation is that for all catalyst distributions, the cumulative emissions decrease very slowly once the catalyst loading exceeds a critical value ($\approx 1.0 \times 10^{10} \text{ s}^{-1}$ in this case). The reason for this can be seen in Fig. 5 and Eq. (17). For $t < t_{\text{ign}}$,

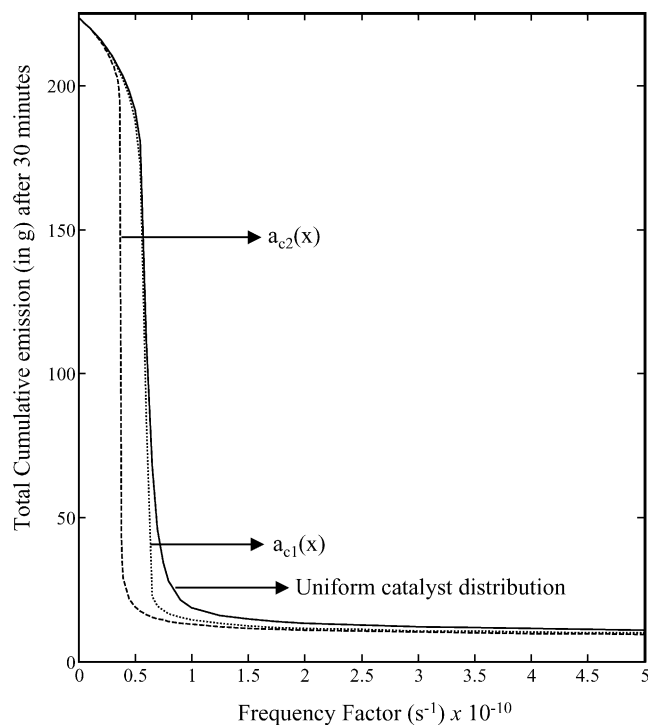


Fig. 8. Cumulative emissions obtained after 30 min as a function of the catalyst loading for different catalyst distributions (with all other parameter values in Table 2).

the emissions are nearly independent of the catalyst loading and this transient period contributes to the emissions.

Another important design parameter discussed in the previous section was the washcoat thickness (δ_c). Fig. 9 shows a plot of the cumulative emissions for different washcoat thickness for the case of uniform catalyst distribution. For very low washcoat thickness (less than the washcoat thickness required for ignition, $\delta_{c,ign}$), there is no ignition in the monolith and the cumulative emissions are high. As the washcoat thickness increases, initially back-end ignition is favored (the transient time is high and steady-state exit conversion is low) and the nature of ignition shifts to middle ignition (with moderate transient time and moderate steady-state exit conversion) and for high values of washcoat thickness, front-end ignition is favored (transient time is low and steady-state exit conversion is high). This behavior is easily seen in Fig. 9. For $\delta_c = 10 \mu\text{m}$, there is no ignition in the monolith and for $\delta_c = 17$ and $20 \mu\text{m}$, back-end ignition is favored and for $\delta_c = 30$ and $50 \mu\text{m}$, middle ignition is favored. For washcoat thickness values higher than $80 \mu\text{m}$ front-end ignition is favored. But as the washcoat thickness is increased further, the transient time keeps decreasing until a critical washcoat thickness ($\delta_{c,opt}$) is reached. Beyond this critical washcoat thickness, the transient time does not decrease any further because strong diffusional limitations starts to exist in the washcoat and increasing the thickness any further does not improve the performance of the monolith. This critical/optimal washcoat thickness is given by Eq. (27). For the standard set of parameters listed in

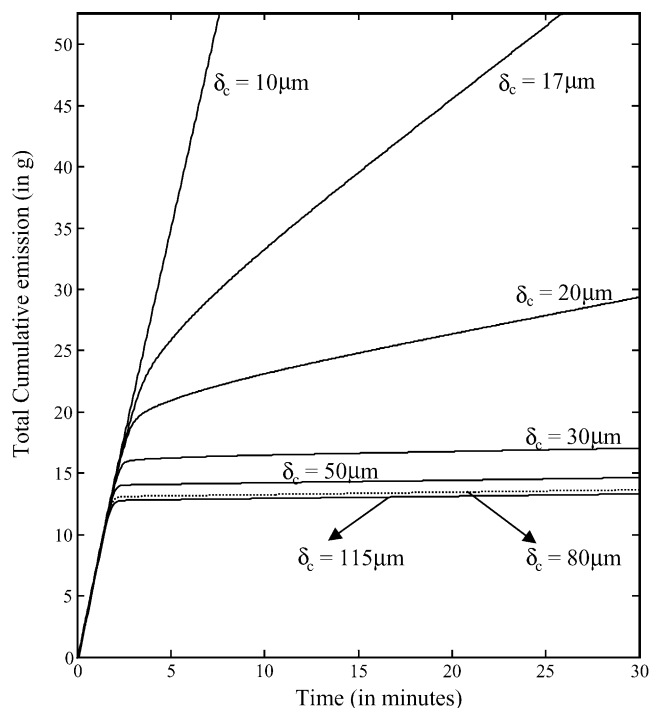


Fig. 9. Cumulative emissions plot for different washcoat thickness and uniform catalyst distribution (with all other parameter values in Table 2).

Table 2 and for uniform catalyst distribution this optimal value of the washcoat thickness is approximately $115 \mu\text{m}$. Though not shown in Fig. 9, for values of washcoat thickness higher than this value, the transient time and cumulative emissions do not decrease any further. Similar behavior can also be seen for the case of nonuniform catalyst loading with more catalyst near the inlet. The only difference that would be observed is that the range of value of washcoat thickness which favors back-end or middle ignition would be very small. Fig. 10 shows the cumulative emissions for the nonuniform catalyst distribution $a_{c1}(x)$. For $\delta_c = 10 \mu\text{m}$, there is no ignition in the monolith and for $\delta_c = 15 \mu\text{m}$, there is a back-end ignition but the ignited length is small and hence the conversion is low. We find a middle ignition (closer to the inlet) for washcoat thickness values of $\delta_c = 16$ and $17 \mu\text{m}$. Front-end ignition (along with good steady-state exit conversion) is favored when the washcoat thickness is greater than $20 \mu\text{m}$. The critical or optimal washcoat thickness for this case is approximately $70 \mu\text{m}$ and for washcoat thickness values greater than this optimal value, the improvement in the performance of the monolith is negligible.

Fig. 11 shows the influence of washcoat thickness on the cumulative emissions for different catalyst distributions. The cumulative emissions obtained after $t = 30$ min is shown as a function of the washcoat thickness for different catalyst distributions. For the case of uniform catalyst distribution, there is no ignition till approximately $15 \mu\text{m}$. As the washcoat thickness is increased beyond this critical

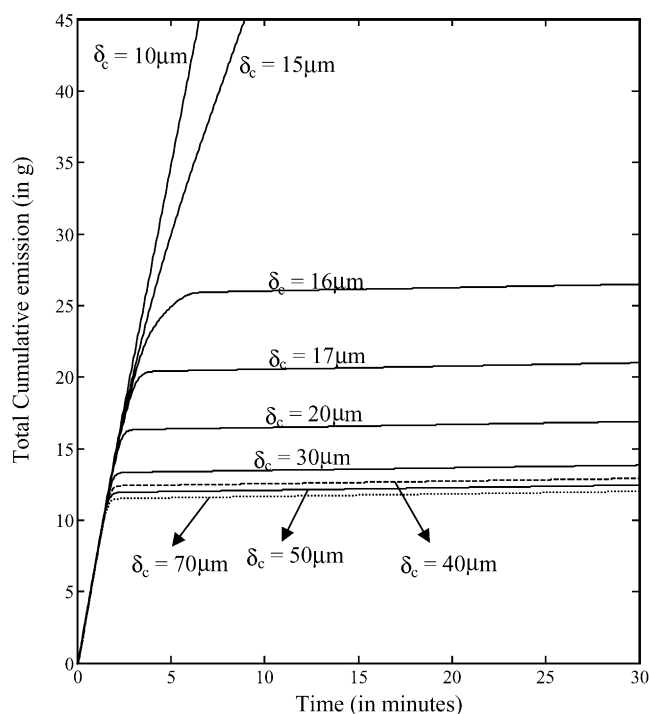


Fig. 10. Cumulative emissions plot for different washcoat thickness and catalyst distribution $a_{c1}(x)$ (with all other parameter values in Table 2).

value, initially back-end ignition is favored and as δ_c increases further, middle ignition is favored followed by front-end ignition. The cumulative emissions (and the transient) time keeps decreasing and as can be seen the cumulative emissions does not decrease any further beyond the optimal washcoat thickness (approximately 115 μm). For the two-zone catalyst distributions, the minimum washcoat thickness required for ignition is lower and are 14 and 10 μm for the catalyst distributions $a_{c1}(x)$ and $a_{c2}(x)$, respectively. For the two-zone distributions, since there is more catalyst near the inlet, range of values of the washcoat thickness that favors back-end ignition is small compared to the uniform distribution case.

We now consider the transient and propagation times in the monolith. For the simulations with front-end ignition, it is easily verified that the transient time obtained from Eq. (29) matches very well with the simulations. Fig. 12 shows a plot of the transient time obtained as a function of $A_r a_c(0)$ for different values of the initial solid temperature for both the typical FTP cycle and for a constant inlet fluid temperature. As the catalyst loading near the inlet ($A_r a_c(0)$) increases, the transient time keeps decreasing and after a certain value, the transition time becomes zero. This is because after a certain catalyst loading, the transition temperature (obtained by solving Eq. (40)) becomes very close to the initial solid temperature. The figure shows the influence of the catalyst loading on the transient time for cases where the inlet fluid temperature changes according to the FTP cycle and for cases where the inlet fluid temperature remains a constant at 600 K. As expected, as the initial solid

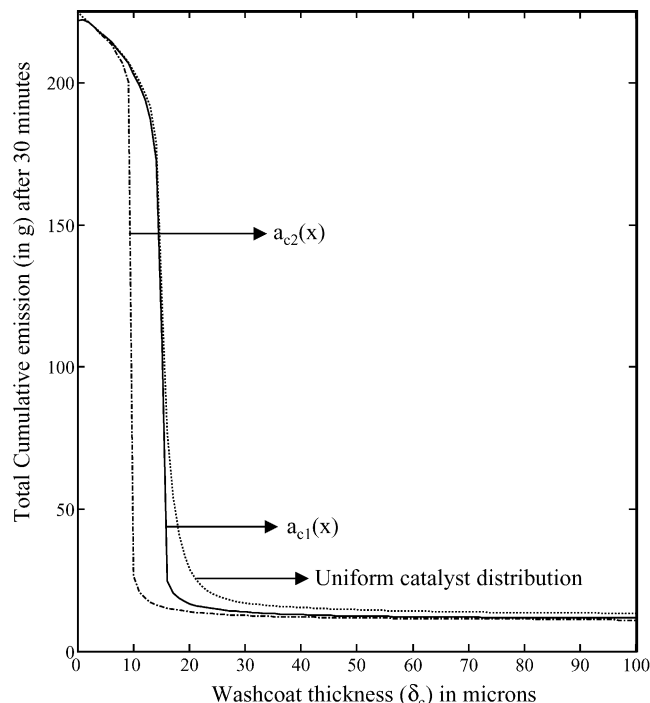


Fig. 11. Cumulative emissions obtained after 30 min as a function of the washcoat thickness for different catalyst distributions (with all other parameter values in Table 2).

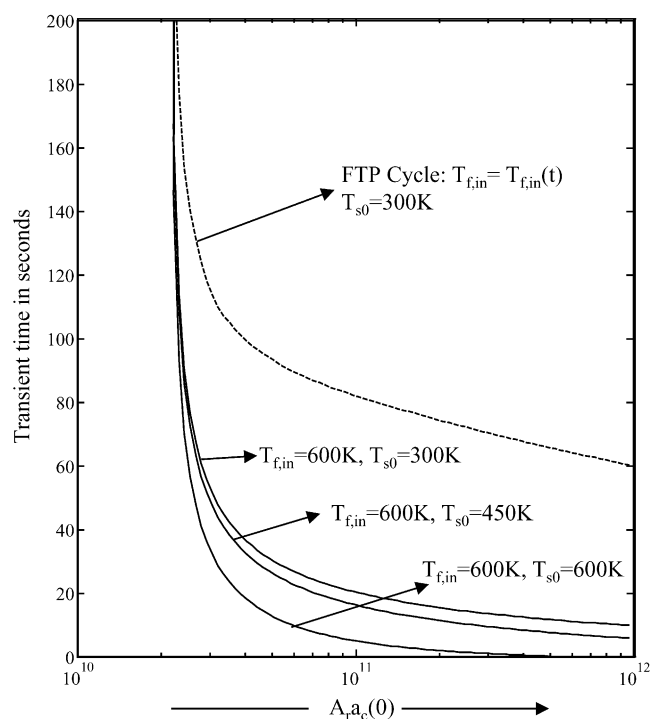


Fig. 12. Transient time shown as a function of the catalyst loading at the inlet [$A_r a_c(0)$] for different initial solid temperatures and for the FTP cycle and constant inlet fluid temperature case (with all other parameter values in Table 2).

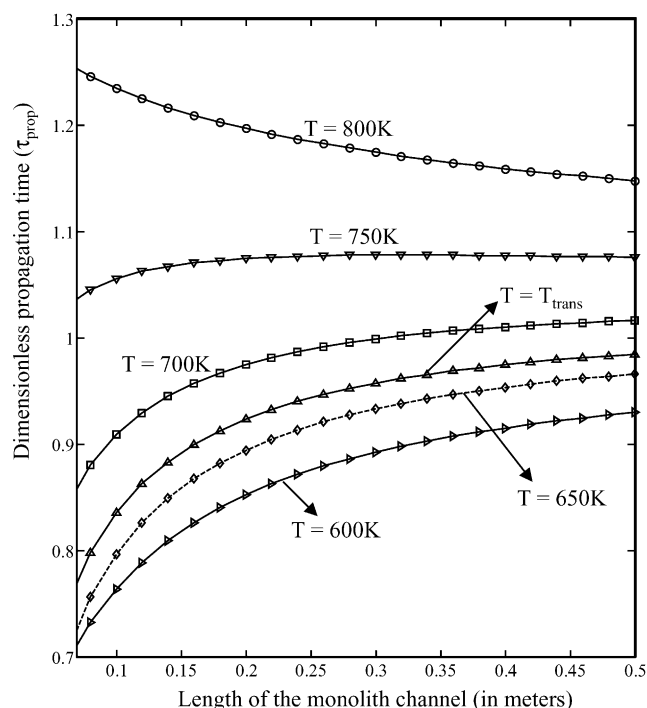


Fig. 13. Dimensionless propagation time shown as a function of the channel length for different solid temperatures for $A_r = 9.6 \times 10^{10} \text{ s}^{-1}$ (with all other parameter values in Table 2).

temperature increases the transient time decreases. Also, since the FTP cycle takes approximately 80 s to reach an inlet fluid temperature of 600 K, the transient time for this case is much higher than for the case of constant inlet fluid temperature.

To analyze the accuracy of the propagation time given by Eq. (33), simulations are carried out for different channel lengths and the propagation time (for different temperatures) is plotted. Fig. 13 shows the dimensionless propagation time for different channel lengths. The different curves in the figure represent the propagation time for different temperatures including the transition temperature ($T_{s,trans}$), which is approximately 670 K for the standard set of parameters used with $A_r = 9.6 \times 10^{10}$. A high value of A_r (or k_{v0}) is chosen so that front-end ignition is favored. [The time taken by the reactor to reach that specified temperature at the exit after the inlet reaches that specified temperature is plotted for different channel length and different temperatures.] As can be seen the dimensionless propagation time is of the order of unity (and ranges between 0.8 and 1.2). As said earlier, for small transverse Peclet numbers (larger channel length) the propagation time is much closer to unity than for large transverse Peclet numbers. If there is no solid conduction, then the propagation time does not depend on the reaction kinetics but for very low solid conduction the dependence of the propagation time on the front velocity is significantly small. Hence, for all practical purposes, to arrive at a reasonably accurate propagation time Eqs. (33) or (34) is sufficient.

Hence, for an optimal design of catalytic converters, front-end ignition (which can be predicted using Eq. (20)) should be favored in the converter by redistributing the catalyst appropriately, the entire monolith should be in the mass transfer controlled regime (as given by Eq. (25)) and the transient time (t_{trans}) and the propagation time (t_{prop}), given by Eqs. (29) and (33) should be as small as possible.

9. Discussion

The cumulative emissions from a catalytic converter depends on both the initial transient period and the steady-state exit concentration. Cumulative emissions can be minimized by reducing the transient time and increasing the steady-state conversion. Though there are other design parameters (such as the solid conductivity, channel geometry, channel dimensions) that could be manipulated to contribute towards optimal design, our focus in this work was limited to studying the effect of the catalyst loading, the catalyst distribution along the channel length and the average thickness of the washcoat on the cumulative emissions. We presented design criteria and showed that by redistributing a fixed amount of catalyst appropriately, we could achieve better transient and good steady-state performances. A two-zone catalyst distribution with more catalyst near the inlet reduces the cumulative emissions substantially compared to the case of uniform catalyst loading. The design criteria and numerical simulations presented here also show that there is an optimal washcoat thickness and/or catalyst loading beyond which the performance of the converter does not improve substantially. Below this optimal washcoat thickness, the transient time is usually high and hence the cumulative emissions are higher.

The design criteria as well as the numerical results presented here (e.g. Figs. 5 and 12) indicate that a significant part of the cumulative emissions come during the initial period $t = 0$ to $t = t_{ign}$ (kinetic regime). As shown here, this ignition time is insensitive to the catalyst loading or washcoat thickness provided these exceed some critical values. Thus, further reduction of t_{ign} requires other strategies such as heating the inlet gas (during the first 60–100 s) or coupling the converter operation to the cold-start engine operation. While electrical heating of the monolith is considered in earlier studies [16], our results in figure 12 indicate that the heating of the inlet gas is more efficient (and perhaps more practical) than heating the solid. [This is because of front-end ignition and very efficient heat transfer between gas and solid near the inlet to the monolith.]

The main results of this work can be extended easily to nonlinear kinetics and multiple reactions as in the case of three-way converters. We note that the steady-state conversion of each species (in the mass transfer controlled regime) can be calculated from Eq. (18) and depends only on the species inlet concentration and diffusivity in the gas phase. Likewise, the temperature front propagation time (for

front-end ignition) is independent of the kinetics and remains the same. However, the ignition time as well as the ignition criterion change and their modifications can be obtained by replacing the heat generation rate for single reaction:

$$Q = (-\Delta H_R) a_c(x) R_v(C_s, T_s) \delta_c \eta$$

by the heat generation rate for multiple reactions

$$Q_{\text{multiple}} = \sum_{i=1}^{N_R} (-\Delta H_R)_i a_c(x) R_{v_i}(C_s, T_s) \delta_c \eta_i$$

and η_i can be found by solving the washcoat diffusion–reaction problem. Thus, with this modification of t_{ign} , the results presented here are applicable to the more general case and the qualitative features and optimal design criteria presented here are not expected to change. A complete analysis of the three-way converter with detailed kinetics will be presented in a future publication.

Acknowledgements

This work was supported by grants from the Robert A. Welch Foundation, Texas Advanced Technology Program and The Dow Chemical Company.

References

- [1] L.L. Hegedus, Temperature excursions in catalytic monoliths, *AIChE J.* 21 (1975) 849.
- [2] R.H. Heck, J. Wei, J.R. Katzer, Mathematical modeling of monolithic catalysts, *AIChE J.* 22 (1976) 477.
- [3] L.C. Young, B.A. Finlayson, Mathematical models of monolith catalytic convertors, *AIChE J.* 22 (1976) 331–353.
- [4] M.A.M. Boersma, W.H.M. Tielen, H.S. Van Der Baan, Experimental and theoretical study of simultaneous development of the velocity and concentration profiles in the entrance region of a monolithic converter, *ACS Symp. Ser.* 65 (1978) 72–82.
- [5] A. Cybulski, J.A. Moulijn, Monoliths in heterogeneous catalysis, *Catal. Rev.: Sci. Eng.* 36 (1994) 179.
- [6] G. Groppi, E. Tronconi, P. Forzatti, Mathematical models of catalytic combustors, *Catal. Rev.: Sci. Eng.* 41 (1999) 227.
- [7] E.G. Becker, C.J. Pereira (Eds.), *Computer Aided Design of Catalysts*, Marcel Dekker, New York, 1993.
- [8] R.E. Hayes, S.T. Kolaczkowski, *Introduction to Catalytic Combustion*, Gordon and Breach Science, The Netherlands, 1997.
- [9] G. Groppi, A. Belloli, E. Tronconi, P. Forzatti, A comparison of lumped and distributed models of monolithic catalytic combustors, *Chem. Eng. Sci.* 50 (1995) 2705.
- [10] E. Tronconi, P. Forzatti, Adequacy of lumped parameter models for SCR reactors with monolithic structures, *AIChE J.* 38 (1992) 201.
- [11] S.H. Oh, J.C. Cavendish, Transients of monolithic catalytic converters: responses to step changes in feed stream temperature as related to controlling automobile emissions, *Ind. Eng. Chem. Prod. Res. Dev.* 21 (1982) 29.
- [12] C.P. Please, P.S. Hagan, D.W. Schwendeman, Light-off behavior of catalytic converters, *SIAM J. Appl. Math.* 54 (1994) 72.
- [13] T. Kirchner, G. Eigenberger, On the dynamic behavior of automotive catalysts, *Catal. Today* 38 (1997) 3.
- [14] D.T. Leighton, H.-C. Chang, A theory for fast igniting catalytic converters, *AIChE J.* 41 (1995) 1898.
- [15] J.M. Keith, H.-C. Chang, D.T. Leighton, Designing a fast-igniting catalytic converter system, *AIChE J.* 47 (2001) 650.
- [16] T. Kirchner, G. Eigenberger, Optimization of the cold-start behavior of automotive catalysts using an electrically heated pre-catalyst, *Chem. Eng. Sci.* 51 (1996) 2409.
- [17] K. Ramanathan, V. Balakotaiah, D.H. West, Light-off criterion and transient analysis of catalytic monoliths, *Chem. Eng. Sci.* 58 (2003) 1381.
- [18] A. Psyllos, C. Philippopoulos, Modelling of monolithic converters with axial catalyst distribution, *Appl. Math. Model.* 17 (1993) 459.
- [19] V. Cominos, A. Gavrilidis, Theoretical investigation of axially non-uniform catalytic monoliths for methane combustion, *Chem. Eng. Sci.* 56 (2001) 3455.
- [20] K. Ramanathan, V. Balakotaiah, D.H. West, Bifurcation analysis of catalytic monoliths with nonuniform catalyst loading, *Ind. Eng. Chem. Res.* 43 (2004) 288.
- [21] S. Tronci, R. Baratti, A. Gavrilidis, Catalytic converter design for minimisation of cold-start emissions, *Chem. Eng. Commun.* 173 (1999) 53.
- [22] K. Ramanathan, D.H. West, V. Balakotaiah, Light-off and cumulative emissions in catalytic monoliths with nonuniform catalyst loading, *Ind. Eng. Chem. Res.* 43 (2004) 4668.
- [23] N. Gupta, V. Balakotaiah, Heat and mass transfer coefficients in catalytic monoliths, *Chem. Eng. Sci.* 56 (2001) 4771.
- [24] V. Balakotaiah, D.H. West, Shape normalization and analysis of the mass transfer controlled regime in catalytic monoliths, *Chem. Eng. Sci.* 57 (2002) 1269.
- [25] R.K. Shah, A. London, *Laminar Forced Convection in Ducts*, Academic Press, New York, 1978.
- [26] S.H. Oh, J.C. Cavendish, Mathematical modeling of catalytic converter lightoff. III. Prediction of vehicle exhaust emissions and parametric analysis, *AIChE J.* 31 (1985) 943.
- [27] C.J. Bennett, S.T. Kolaczkowski, W.J. Thomas, Determination of heterogeneous reaction kinetics and reaction rates under mass transfer controlled conditions for a monolith reactor, *Trans. Inst. Chem. Eng., Part B* 69 (1991) 209–220.